

Idealized simulations
of pyro-convective
clouds

P. Reutter et al.

3-D model simulations of dynamical and microphysical interactions in pyro-convective clouds under idealized conditions

P. Reutter^{1,2}, J. Trentmann³, A. Seifert³, P. Neis^{1,2}, H. Su¹, M. Herzog⁴, H. Wernli⁵, M. O. Andreae¹, and U. Pöschl¹

¹Max Planck Institute for Chemistry, Biogeochemistry Department, Mainz, Germany

²Institute for Atmospheric Physics, Johannes Gutenberg-University, Mainz, Germany

³Deutscher Wetterdienst, DWD, Offenbach, Germany

⁴Department of Geography, University of Cambridge, United Kingdom

⁵ETH Zurich, Switzerland

Received: 28 June 2013 – Accepted: 5 July 2013 – Published: 23 July 2013

Correspondence to: P. Reutter (preutter@uni-mainz.de)

Published by Copernicus Publications on behalf of the European Geosciences Union.

Title Page

Abstract

Introduction

Conclusions

References

Tables

Figures

◀

▶

◀

▶

Back

Close

Full Screen / Esc

Printer-friendly Version

Interactive Discussion



Abstract

Pyro-convective clouds, i.e. convective clouds forming over wildland fires due to high sensible heat, play an important role for the transport of aerosol particles and trace gases into the upper troposphere and lower stratosphere. Additionally, due to the emission of a large number of aerosol particles from forest fires, the microphysical structure of a pyro-convective cloud is clearly different from that of ordinary convective clouds.

A crucial step in the microphysical evolution of a (pyro-) convective cloud is the activation of aerosol particles to form cloud droplets. The activation process affects the initial number and size of cloud droplets and can thus influence the evolution of the convective cloud and the formation of precipitation.

Building upon a realistic parameterization of CCN activation, the model ATHAM is used to investigate the dynamical and microphysical processes of idealized three-dimensional pyro-convective clouds in mid-latitudes. A state-of-the-art two-moment microphysical scheme has been implemented in order to study the influence of the aerosol concentration on the cloud development.

The results show that the aerosol concentration influences the formation of precipitation. For low aerosol concentrations ($N_{\text{CN}} = 1000 \text{ cm}^{-3}$), rain droplets are rapidly formed by autoconversion of cloud droplets. This also triggers the formation of large graupel and hail particles resulting in an early and strong onset of precipitation. With increasing aerosol concentration ($N_{\text{CN}} = 20000 \text{ cm}^{-3}$ and $N_{\text{CN}} = 60000 \text{ cm}^{-3}$) the formation of rain droplets is delayed due to more but smaller cloud droplets. Therefore, the formation of ice crystals and snowflakes becomes more important for the eventual formation of graupel and hail. However, this causes a delay of the onset of precipitation and its intensity for increasing aerosol concentration.

This work shows the first detailed investigation of the interaction between cloud microphysics and dynamics of a pyro-convective cloud using the combination of a high resolution atmospheric model and a detailed microphysical scheme.

ACPD

13, 19527–19557, 2013

Idealized simulations of pyro-convective clouds

P. Reutter et al.

Title Page

Abstract

Introduction

Conclusions

References

Tables

Figures

◀

▶

◀

▶

Back

Close

Full Screen / Esc

Printer-friendly Version

Interactive Discussion



**Idealized simulations
of pyro-convective
clouds**P. Reutter et al.

[Title Page](#)[Abstract](#)[Introduction](#)[Conclusions](#)[References](#)[Tables](#)[Figures](#)[Back](#)[Close](#)[Full Screen / Esc](#)[Printer-friendly Version](#)[Interactive Discussion](#)

important parameter influencing the Chisholm pyro-cumulonimbus, which is also consistent with other studies (Penner et al., 1986; Lavouè et al., 2000). When more sensible heat is available the cloud is reaching higher altitudes, thereby condensing and freezing more of the available water and releasing additional latent heat, which gives rise to a positive feedback. The sensitivity simulations of the Chisholm pyro-cloud on the aerosol concentration showed that the updraft region is only weakly affected by the aerosol loading is in contrast to the findings of other studies, which reported a stronger convection with increasing aerosol concentration (Andreae et al., 2004; Koren et al., 2005). The reported invigoration of deep convection with increasing aerosol concentration has been explained by a delay in the formation of precipitation and the suppression of downdrafts and warm rain (Andreae et al., 2004; Koren et al., 2005; Rosenfeld et al., 2008). Therefore, more liquid condensate reaches higher altitudes releasing more latent heat upon freezing. The additional latent heat release leads to an invigoration of the convection. Another aspect of cloud modification by aerosols concerns the cloud life time. Lindsey and Fromm (2008) showed that the highly polluted anvil of a pyro-Cb persisted 6–12 h longer than convectively-generated cirrus anvils from clean convection in the vicinity of the pyro-Cb. Thus, pyro-convective clouds are a unique form of atmospheric convection in terms of microphysical and dynamical properties, which makes them an ideal test bed for investigations of aerosol-cloud interactions.

In this study we focus on the influence of the aerosol number concentration on the microphysical structure and dynamical development of an idealized pyro-convective cloud. A crucial step in the microphysical evolution of a convective cloud is the activation of aerosol particles to form cloud droplets. The activation process affects the initial number and size of cloud droplets and can thus influence the progression of the convective cloud and the formation of precipitation. Although several studies in past years were able reproduce the dynamical evolution of pyro-convective clouds well (Trentmann et al., 2006; Cunningham and Reeder, 2009), the activation of aerosol particles to cloud droplets was either neglected (Cunningham and Reeder, 2009) or parameterized in a strongly simplified way (Trentmann et al., 2006). In this study we improve

the description of aerosol activation by the introduction of a look-up table specially obtained for pyro-convective conditions using realistic aerosol size distributions and chemical properties (Reutter et al., 2009). This enables the microphysical scheme to simulate the aerosol activation in a more realistic way. For the first time, the interaction between microphysics and dynamics within a pyro-convective clouds can be studied in detail within a three-dimensional high resolution model.

This paper is organised as follows. In the next section the ATHAM model and the setup of the experiments are described. This is followed in Sect. 3 by the presentation and discussions of the results of sensitivity studies with three different aerosol concentrations.

2 Model description

The three-dimensional model ATHAM (Active Tracer High resolution Atmospheric Model) is able to simulate intense forms of atmospheric convection induced by volcanic eruptions or intense forest fires (Oberhuber et al., 1998; Graf et al., 1999; Textor et al., 2006; Tupper et al., 2009). The model solves the complete Navier-Stokes equations including sound waves, which cannot be excluded due to the possible supersonic flow around the vent of a volcano. The model also contains the equation for tracer advection. The equations are solved with an implicit time stepping scheme on a staggered Arakawa C grid (Arakawa and Lamb, 1977). This grid allows stretching for the use of a higher spatial resolution in regions where strong gradients can occur, e.g. in the vicinity of the fire. The dynamical core of ATHAM takes the effects of active tracers into account. An active tracer in this framework is defined as a component that affects the density, heat capacity and compressibility of the air in the model. In this study, all hydrometeors as well as the aerosol particles are treated as active tracers. For the representation of sub-grid processes a prognostic turbulence scheme is implemented (Herzog et al., 2003), which allows to differentiate between horizontal and vertical turbulent exchange processes when anisotropy in turbulence cannot be ignored.

Idealized simulations of pyro-convective clouds

P. Reutter et al.

Title Page

Abstract

Introduction

Conclusions

References

Tables

Figures



Back

Close

Full Screen / Esc

Printer-friendly Version

Interactive Discussion



**Idealized simulations
of pyro-convective
clouds**

P. Reutter et al.

Title Page

Abstract

Introduction

Conclusions

References

Tables

Figures

◀

▶

◀

▶

Back

Close

Full Screen / Esc

Printer-friendly Version

Interactive Discussion



For the calculation of microphysical processes within the pyro-convective clouds in this study the two-moment mixed-phase bulk microphysical parameterization of Seifert and Beheng (2006) (SB scheme hereafter) has been implemented. It comprises the six hydrometeor categories cloud water, rain water, cloud ice, snow, graupel and hail. For each category mass and number densities are prognostic variables. For a description of this scheme see also Blahak (2008) and Noppel et al. (2010). The information on the number and mass of the hydrometeors is essential for this study in order to simulate the indirect aerosol effects (Lohmann and Feichter, 2005) on the pyro-convective clouds. The realization of the cloud droplet nucleation in the SB scheme had to be modified compared to the original version to achieve a realistic description of the cloud formation of pyro-convective clouds. For the nucleation of cloud droplets the model uses a look-up table based on the aerosol activation study by Reutter et al. (2009), which investigated the formation of cloud droplets under pyro-convective conditions using a parcel model with detailed spectral description of cloud microphysics. It was found that, depending on the ratio between updraft velocity and aerosol concentration different regimes of cloud droplet formation occur. Hence, with the knowledge of the updraft velocity at the cloud base and the aerosol number concentration, the number of newly formed cloud droplets can be estimated through a look-up table. This table is characteristic for an aerosol size distribution with a mean diameter of 120 nm, a geometric standard deviation of $\sigma_g = 1.5$ (Reid et al., 2005) and an effective hygroscopicity parameter of 0.2 (Petters and Kreidenweis, 2007; Andreae et al., 2008), which are typical values for young biomass burning aerosol. The required parameters for the lookup-table are the updraft velocity w and the number of aerosol particles N_{CN} . Therefore, for each horizontal grid point the updraft velocity at the cloud base must be identified in the ATHAM simulation.

The cloud base in ATHAM is detected when the following criteria are fulfilled: (1) the updraft velocity w has to be larger than 0.1 ms^{-1} , (2) the supersaturation S has to be larger than 0% and (3) the supersaturation at the next-lower model level has to be smaller than the supersaturation in the current model level. Most likely the updraft

velocity at this location does not correspond exactly to a value in the lookup-table, hence a linear interpolation is made between two tabulated values. In the model version used for this study, the lookup-table has entries for nine different updraft velocities (1, 2.5, 5, 7, 10, 12, 15, 17 and 20 ms^{-1} , see Table 1).

For the sensitivity studies regarding the aerosol particle concentration N_{CN} , a fixed value of N_{CN} is used for all grid points where the nucleation is calculated. The advantage of this method is that an exact number of N_{CN} can be prescribed, which is useful for idealized sensitivity studies. Note, that N_{CN} in the model is only used for the activation of cloud droplets and therefore has no influence on other parameters. Also, the scavenging of aerosol particles by nucleation and impaction scavenging is not implemented in this version of ATHAM.

The model runs were initialized with a mid-latitude US standard atmosphere with no background wind. The model domain was set to 40 km \times 30 km \times 20 km with 110 \times 80 \times 55 grid points in the x - y - z -directions, respectively. The minimum horizontal and vertical grid box size was set to 50 m at the centre of the domain where the fire was located. Due to the stretched grid, the size of the grid boxes increases towards the borders of the model domain. The size of the fire front was set to 316 m \times 316 m and the energy release from the fire was calculated following Trentmann et al. (2006) with a fuel loading of 9 kg m^{-2} and a value of 18700 kJ kg^{-1} for the standard heat of combustion (ASRD, 2001), which corresponds to a fire forcing of 378 kW m^{-2} . Within the first minute of the simulation, the fire forcing is linearly increased from zero to the final fire forcing. After 60 min, the fire forcing is shut down linearly to zero within one minute. For the aerosol emissions, we used an emission factor of 9.1 $\text{g kg}_{\text{fuel}}^{-1}$ (Andreae and Merlet, 2001). The time step was set automatically between 0.5 s and 1.5 s in order to fulfil the Courant-Friedrichs-Levy criterion.

For the following studies the aerosol number concentration for the activation of cloud droplets was set to three different cases: (i) a clean case with $N_{\text{CN}} = 1000 \text{ cm}^{-3}$, (ii) an intermediate case with $N_{\text{CN}} = 20000 \text{ cm}^{-3}$ and (iii) a strongly polluted case with $N_{\text{CN}} = 60000 \text{ cm}^{-3}$. Note that the aerosol particle concentration of case (i) is unrealistic

Idealized simulations of pyro-convective clouds

P. Reutter et al.

Title Page

Abstract

Introduction

Conclusions

References

Tables

Figures



Back

Close

Full Screen / Esc

Printer-friendly Version

Interactive Discussion



for pyro-convective conditions. However, this case provides a good basis of comparison for the influence of aerosol particles on the evolution of pyro-convective clouds.

3 Results

The aim of this study is to investigate the sensitivity of the microphysical and dynamical structure of a pyro-convective cloud on aerosol concentrations representing clean, intermediate and strongly polluted conditions. First, we analyse the dynamical evolution and the transport of smoke. After that, the microphysical differences between the different aerosol conditions are investigated.

3.1 Dynamical evolution

Figure 1 shows the temporal evolution of the number of cloudy grid points, which is a measure for the size of the pyro-clouds, for the different aerosol particle concentrations. The results show the most rapid development in terms of size for the clean case, while the strongly polluted case is characterized by a comparatively slow evolution. After ca. 60 min, all three pyro-clouds show the same number of cloudy grid points. At this time, the fire is shut down and the external forcing driving convection is removed. No clear signal of the shutdown of the fire is visible in Fig. 1. The increase in the number of cloudy grid points or the rain rate shows no discontinuity due to the shutdown of the fire. However, it appears that in all three cases the cloud has reached its maximum size after about 90 min in terms of the number of cloudy grid points, with the largest size for the strongly polluted case and the smallest size for the clean case. In contrast, the rainrate is largest for the clean case after 90 min and smallest for the strongly polluted case. This indicates that the dynamical evolution of a strongly polluted pyro-convective cloud is limited in the beginning, but more sustainable, pointing to a cloud lifetime effect resulting from the higher aerosol loading (Lohmann and Feichter, 2005).

Idealized simulations of pyro-convective clouds

P. Reutter et al.

Title Page

Abstract

Introduction

Conclusions

References

Tables

Figures



Back

Close

Full Screen / Esc

Printer-friendly Version

Interactive Discussion



Idealized simulations of pyro-convective clouds

P. Reutter et al.

Title Page

Abstract

Introduction

Conclusions

References

Tables

Figures

◀

▶

◀

▶

Back

Close

Full Screen / Esc

Printer-friendly Version

Interactive Discussion



Interestingly, from a dynamical point of view, the clean and intermediate polluted cases show a very similar behaviour. The only noteworthy difference is that the clean case shows an earlier onset of the rapid evolution (~ 5 min) than the intermediate polluted case. This rapid evolution is triggered by the latent heat release, when large amounts of cloud and rain droplets freeze and form ice crystals, snow and hail. This additional latent heat results in a higher updraft velocity and hence in a more rapid growth of the pyro-convective cloud (Rosenfeld et al., 2008). However, a different pattern is seen concerning the precipitation rate. Here, the intermediate and strongly polluted case show a similar behaviour, and both have a significantly reduced (\sim factor of 2) rain rate compared to the clean case. This will be examined in detail in Sect. 3.2.

Another measure for the dynamical evolution of a pyro-convective cloud is the vertical distribution of aerosol mass. Figure 2 shows the averaged vertical distribution for the three cases after 30, 60 and 90 min, respectively. Note, that the different aerosol concentrations are only used for the activation of the cloud droplets and have no influence on the aerosol mass, which is emitted by the fire. Therefore, the emitted mass by the fire is equal for all three cases. After 30 min the height of the maximum of the aerosol mass distribution (h_{aero}) is highest for the cleanest case ($h_{\text{aero}} = 9600$ m), followed by the two polluted cases ($h_{\text{aero}} = 8900$ m). After 60 min the amount of aerosol mass at h_{aero} increases similarly for all cases, while h_{aero} is increasing for the intermediate case to 9600 m and staying constant for the other two cases. 90 min after ignition of the fire h_{aero} is equal for all three cases (9600 m) and the amount of aerosol mass differs only marginally. This result is in very good agreement with the sensitivity study by Luderer et al. (2006). The height of the cloud top shows a similar evolution and reaches its maximum after 90 min at 12 100 m for all three cases. These results show that the aerosol loading only weakly affects the cloud top height.

3.2 Microphysical evolution

The temporal evolution of the total liquid and frozen water content (in g kg^{-1}) averaged over the complete model domain is shown in Fig. 3 in order to investigate the differ-

Idealized simulations of pyro-convective clouds

P. Reutter et al.

Title Page

Abstract

Introduction

Conclusions

References

Tables

Figures

◀

▶

◀

▶

Back

Close

Full Screen / Esc

Printer-friendly Version

Interactive Discussion



ences in the microphysics due to the differing aerosol loadings. It can be seen that the appearance for the six hydrometeor classes (cloud droplets, rain, ice particles, snow, graupel, and hail) is different for the three cases. In the clean case ($N_{CN} = 1000\text{cm}^{-3}$) the formation of rain droplets is the first process after the activation of cloud droplets.

This is followed by the production of ice crystals, snow, and graupel, respectively. The last hydrometeor class to appear is hail. During the first hour of the simulation, the largest hydrometeor class in terms of average water content is graupel. At the end of the simulation, rain, hail and graupel are the dominant hydrometeor classes regarding the water mass within the pyro-convective cloud. In the intermediate case ($N_{CN} = 20000\text{cm}^{-3}$) the activation of cloud droplets is also followed by the formation of rain droplets. However, after an initial production phase, the rain droplet formation stagnates for about 20 min and only afterwards rain droplets are produced in a significant amount. After the initial production of rain, ice crystals develop, followed by snow and graupel, respectively. Again, hail is the last hydrometeor class to appear. At the end of the intermediate case, rain, graupel and hail are the dominant hydrometeors. However, throughout most of the simulation time, graupel is the hydrometeor class that contains the greatest water mass. In the strongly polluted case ($N_{CN} = 60000\text{cm}^{-3}$) the formation of significant amount of rain, graupel and hail is clearly delayed and separated from the formation of ice crystals and snow, where snow is the dominant hydrometeor class within the first hour of the simulation.

In Fig. 4 the y - z cross sections at $x = 0\text{km}$ of the three different pyro-convective clouds after 60 min show (colour coded) the water content in gkg^{-1} and (red contour) the $0.1\ \mu\text{gkg}^{-1}$ isoline of the interstitial aerosol describing the shape of the smoke plume for (top row) all hydrometeors, (middle row) the liquid phase and (bottom row) the frozen phase. The black lines denote the 0°C , 0 – 20°C and -40°C isotherms, respectively. The results show that the aerosol concentration has an influence on the distribution of water within the cloud and also on the precipitation. The strongest maximum of the total hydrometeor content can be found in the clean case, where in the updraft region values of up to 9.5gkg^{-1} are visible. Also in this case the strongest pre-

**Idealized simulations
of pyro-convective
clouds**

P. Reutter et al.

Title Page

Abstract

Introduction

Conclusions

References

Tables

Figures

◀

▶

◀

▶

Back

Close

Full Screen / Esc

Printer-friendly Version

Interactive Discussion



5 precipitation pattern of all three cases can be observed, even within the updraft region of the cloud, which indicates large rain droplets. With increasing aerosol concentration the maximum hydrometeor content and the amount of precipitation is decreasing, while the hydrometeor content in the outer regions of the cloud is significantly increased. The middle row of Fig. 4 also shows that the liquid particles (cloud and rain droplets) reach an maximum altitude of about 8600 m for the clean case and about 9500 m for the strongly polluted case. It also can be seen that the precipitation reaching the ground consists purely of rain droplets. Note that this rain is partially formed by precipitating graupel and hail particles, which are melting to rain droplets after they cross the 0°C isoline. To understand the distribution of the liquid and frozen water, the composition of the cloud is discussed in more detail for each case.

10 Figure 5 shows an y - z -cross section of the cloud and rain water content for each case. Here it can be clearly seen that the cloud water content is increasing with increasing aerosol pollution, while the rain water content shows the opposite effect, which can be explained by the number and size of the cloud droplets. For the clean case the cloud droplet number is low and therefore the mean volume radius of the cloud droplets is large (up to 20 μm , see Appendix), which allows a fast transition to rain droplets by autoconversion and accretion. Note that in the clean case an important part of the rain formation also occurs by the melting of large frozen particles (hail and graupel), which can be seen by the outer bands of precipitation at $y = \pm 0.5 \text{ km}$ in Fig. 5. Nevertheless, in order to form graupel and especially hail, a sufficient amount of rain droplets is crucial. Therefore, the onset of precipitation in the clean case occurs via the liquid phase. In the intermediate case the cloud water content already is significantly larger and much less rain water is found. The larger amounts of CCN particles lead to more but smaller cloud droplets and therefore the efficiency of autoconversion and accretion is reduced, which leads to a reduction of rain water. In the strongly polluted case the cloud droplets are extremely small (mean volume radius < 6 μm), which leads to an inefficient production of rain droplets by autoconversion or accretion.

**Idealized simulations
of pyro-convective
clouds**

P. Reutter et al.

[Title Page](#)[Abstract](#)[Introduction](#)[Conclusions](#)[References](#)[Tables](#)[Figures](#)[⏪](#)[⏩](#)[◀](#)[▶](#)[Back](#)[Close](#)[Full Screen / Esc](#)[Printer-friendly Version](#)[Interactive Discussion](#)

Figure 6 shows the cross section of the cloud ice and snow water content for the three different aerosol concentrations. Again, large differences between the different aerosol loadings can be observed, with the smallest amount of cloud ice and snow for the clean case. This is consistent with the results for the liquid particles, because in ATHAM cloud ice is formed by freezing of cloud droplets and by nucleation and deposition freezing. In the next step snow is formed by aggregation of cloud ice. Due to the lower amount of cloud droplets in the clean case and hence lower amount of cloud ice, only a small amount of snow is produced. When the aerosol concentration is increased the cloud droplet concentration is also increased and therefore more cloud droplets are transported to heights where they freeze and form cloud ice. This higher production of ice crystals leads also to a higher production of snow. In the strongly polluted case the snow class is the most important particle class within the first hour of the simulation and is spread all across the supercooled regions of the cloud, except in the vigorous updraft region.

Figure 7 shows the water content of the two largest frozen hydrometeor classes, graupel and hail. The clean case shows the largest amounts of water content for graupel and hail, which can be found even at heights where the temperature is above the freezing temperature of water. In this region graupel and hail are melting and transferred to the rain class. It can also be seen that the graupel particles are more horizontally spread than the hail particles, which can be explained by their size. The smaller graupel particles with a mean volume radius of up to $900\ \mu\text{m}$ in the upper regions of the cloud can be transported horizontally before the particles fall down. The hail particles are already that large in the upper parts of the cloud that they start to fall down before they can be transported to the outer regions of the cloud. In the intermediate case, the amount of hail is significantly reduced compared to the clean case, while the amount of graupel is only slightly reduced. The hail formation in the intermediate case is suppressed by the delayed production of rain droplets, although the formation of graupel is similar for the clean and intermediate case. In the strongly polluted case the hail water content after 60 min is very similar compared to the results of the intermediate case.

**Idealized simulations
of pyro-convective
clouds**

P. Reutter et al.

Title Page

Abstract

Introduction

Conclusions

References

Tables

Figures



Back

Close

Full Screen / Esc

Printer-friendly Version

Interactive Discussion

However, the graupel water content in the strongly polluted case is drastically reduced compared to the other two cases. The reason for this is the high concentration of snow particles, which leads to a growth of the graupel particles rather than the formation of new graupel particles. The sizes of the graupel particles in the strongly polluted case are the largest of all three cases with a mean volume radius of up to 1.6 mm, while in the other two cases the largest graupel particles have a mean volume radius of 1 to 1.4 mm. Therefore, the graupel particles in the strongly polluted case start to precipitate and are transferred into the rain class as soon as they reach an altitude with a temperature above 0°C. The production of hail in the strongly polluted case goes alongside the rain formation, which shows a behaviour comparable to the intermediate case. Therefore, the amounts of hail in both cases is comparable.

From the investigations of the dynamical and microphysical properties of the three different cases presented above, the following conclusion can be drawn. After the rapid formation of rain by autoconversion of cloud droplets in the clean case, graupel and hail are formed within a short period of time. This means that already at an early stage of the cloud evolution a significant amount of water is transferred to the frozen phase. This leads to a strong release of latent heat due to the phase transition resulting in a rapid evolution of the cloud (Fig. 1, black line around 700s). On the other hand, the rain droplets, graupel and hail particles grow rapidly and soon start to precipitate beginning 1700s after model start.

In the intermediate case the formation of rain is slower compared to the clean case, because the cloud droplets are smaller. Therefore, the formation of ice crystals and snowflakes triggers the formation of graupel and hence the freezing of large amounts of water by freezing rain droplets is delayed in this case. Hence, the rapid evolution of the intermediate polluted cloud is shifted to a later time (1000s). Because the formation of hail depends on the freezing of large rain droplets, the evolution of hail is also delayed. However, the precipitation starts almost at the same time compared to the clean case, while the precipitation rate is significant smaller.

**Idealized simulations
of pyro-convective
clouds**

P. Reutter et al.

[Title Page](#)[Abstract](#)[Introduction](#)[Conclusions](#)[References](#)[Tables](#)[Figures](#)[Back](#)[Close](#)[Full Screen / Esc](#)[Printer-friendly Version](#)[Interactive Discussion](#)

In the strongly polluted case the formation of rain, graupel and hail is even more delayed compared to the previous cases, because of the very small size of the cloud droplets in this case. This leads to a delay in the freezing of larger amounts of water in the cloud and hence the rapid increase in the size of the cloud is postponed until sufficient amounts of cloud and rain droplets are available for freezing (1250s). Additionally, the onset of precipitation is latest of all three cases and begins after 2400s. Nevertheless, after 1 h of simulation, all clouds show approximately the same size. Therefore, the aerosol concentration has a rather small influence on the size of a mature pyro-convective cloud, but is very important for its microphysical evolution. A key point is the shift in the onset and amount of precipitation with increasing aerosol concentration.

After the shutdown of the fire (60 min after model start) the pyro-convective clouds show no clear response due to the absence of the fire. However, the rain rate for each case is continuously increasing, but remains less for the polluted cases compared to the clean case. This is in agreement with the cloud lifetime effect, which says that smaller cloud droplets decrease the precipitation efficiency and hence prolong the cloud lifetime (Lohmann and Feichter, 2005). Note, that in this model setup we do not take radiative effects into account. However, due to the different microphysical properties of the different cases, a significant change of the radiative effects can be expected (cloud albedo effect). On the other side, this would effect the cloud evolution only weakly.

4 Summary and discussion

In this study the influence of the aerosol concentration on the dynamical and microphysical evolution of a pyro-convective cloud has been investigated. Therefore, a sophisticated two-moment microphysical scheme (Seifert and Beheng, 2006) has been implemented into the cloud-resolving model ATHAM. To study the influence of different aerosol concentrations on pyro-convective clouds a look-up table based on the results

of a cloud droplet activation study (Reutter et al., 2009) was included into the micro-physical scheme.

Sensitivity studies have been conducted with three different aerosol concentrations: (i) a clean case with an aerosol concentration of $N_{\text{CN}} = 1000 \text{ cm}^{-3}$, (ii) an intermediate case with $N_{\text{CN}} = 20000 \text{ cm}^{-3}$ and (iii) a strongly polluted case with $N_{\text{CN}} = 60000 \text{ cm}^{-3}$. After 60 min of model integration the influence of the aerosol concentration on the dynamical evolution of a pyro-convective is rather weak in terms of the size of the cloud and the smoke distribution within the cloud. In contrast, the aerosol concentration has a strong impact on the microphysical evolution of pyro-convective clouds. In the clean case, rain forms rapidly by autoconversion of cloud droplets. Due to the low number concentrations of aerosol particles and the high supersaturation produced by the strong updraft of a pyro-convective cloud, the cloud droplets are large and hence the autoconversion is an efficient process for rain formation. After that ice crystals, snow and graupel are formed within a short period of time. Hence, already at an early stage of the cloud life cycle a significant amount of water is transferred to the frozen phase, which leads to an additional release of latent heat that further intensifies the strong updraft region. The rain droplets, hail and graupel particles are growing fast and soon start to precipitate.

In the intermediate case the formation of rain is slower compared to the clean case. This is due to the fact that the higher aerosol concentration leads to more but smaller cloud droplets, which reduces the efficiency of the autoconversion. Therefore, the formation of ice crystals and snowflakes becomes more important for the eventual formation of graupel and hail. Compared to the clean case the freezing of water is delayed and hence also the rapid growth of the cloud.

In the strongly polluted case the formation of rain, graupel and hail is even more delayed compared to the previous cases, because of the extremely small cloud droplets in this case. In the beginning only cloud droplets, ice crystals and snowflakes can be observed, which leads to the latest formation of precipitation in all three cases.

**Idealized simulations
of pyro-convective
clouds**

P. Reutter et al.

Title Page

Abstract

Introduction

Conclusions

References

Tables

Figures



Back

Close

Full Screen / Esc

Printer-friendly Version

Interactive Discussion



Idealized simulations of pyro-convective clouds

P. Reutter et al.

Title Page

Abstract

Introduction

Conclusions

References

Tables

Figures

◀

▶

◀

▶

Back

Close

Full Screen / Esc

Printer-friendly Version

Interactive Discussion



Overall, after one hour all three cases show the same size of the pyro-convective cloud. At this point, the fire in the model is turned off. Interestingly, the pyro-convective clouds show no clear response to the absence of the fire. In all cases the rain rate is increasing during and after the shutdown of the fire. However, for the intermediate and strongly polluted case the rain rate is significantly smaller compared to the clean case. On the other hand, the size of the cloud after 90 min is largest in the strongly polluted case (cloud lifetime effect).

Overall it can be concluded that the microphysical structure of a pyro-convective cloud is very sensitive to the aerosol concentration in the rising plume, which leads to a delay of precipitation with increasing pollution.

Various studies have shown the different microphysical evolution of clouds for different aerosol concentrations in observational data (Costa et al., 2000; Andreae et al., 2004) and in model simulations (Khain et al., 2005; Seifert and Beheng, 2006; Diehl et al., 2007; Tao et al., 2007; Storer and van den Heever, 2013), which are consistent with the findings of this study. However, in most 3-D model simulations (Khain et al., 2005; Seifert and Beheng, 2006; Tao et al., 2007; Seifert et al., 2012) the sensitivity of the aerosol concentration on the evolution of clouds was studied in a range between $N_{\text{CN}} = 100 \text{ cm}^{-3}$ and $N_{\text{CN}} = 3200 \text{ cm}^{-3}$ with the assumption of a model salt like the very hydrophilic sodium chloride ($\kappa = 1.28$). This is very unrealistic for pyro-convective clouds, because during a biomass-burning event a high number of less hydrophilic particles ($\kappa < 0.6$) are emitted. Admittedly, the sensitivity on the aerosol concentration is larger, when more hydrophilic particles like sodium chloride are used. Therefore, the effect of the pollution on the evolution of a cloud with lower aerosol concentration but higher hygroscopicity is an approximation of highly polluted conditions like in this study. Storer and van den Heever (2013) conducted model simulations with a similar approach of CCN activation using a lookup-table obtained by parcel model simulations. However, they focus on tropical deep convection, which is influenced by aerosol concentrations up to 3200 cm^{-3} , representing Saharan dust events.

For the first time the sensitivity of the aerosol concentration on the evolution of a pyro-convective cloud is studied with a realistic description of the activation of cloud droplets from clean to strongly polluted conditions using activation properties corresponding to freshly emitted biomass burning aerosol.

However, more studies are needed to further improve our understanding of the influence of aerosol concentration on the evolution of pyro-convective clouds, using realistic meteorological conditions to comprise also effects such as background winds or more realistic atmospheric soundings.

Appendix A

Radius

Here, the figures for the radius of the hydrometeors are shown (Figs. A1, A2 and A3).

Acknowledgements. This work has been supported by an International Max Planck Research School fellowship.

The service charges for this open access publication have been covered by the Max Planck Society.

References

- Andreae, M. O. and Merlet, P.: Emission of trace gases and aerosols from biomass burning, *Global Biogeochem. Cy.*, 15, 955–966, 2001. 19533
- Andreae, M. O. and Rosenfeld, D.: Aerosol-cloud-precipitation interactions. Part 1: The nature and sources of cloud-active aerosols, *Earth Sci. Rev.*, 89, 13–41, doi:10.1016/j.earscirev.2008.03.001, 2008. 19532
- Andreae, M. O., Rosenfeld, D., Artaxo, P., Costa, A. A., Frank, G. P., Longo, K. M., and Silva-Dias, M. A. F.: Smoking rain clouds over the Amazon, *Science*, 303, 1337, doi:10.1126/science.1092779, 2004. 19529, 19530, 19542

Idealized simulations of pyro-convective clouds

P. Reutter et al.

Title Page

Abstract

Introduction

Conclusions

References

Tables

Figures

⏪

⏩

◀

▶

Back

Close

Full Screen / Esc

Printer-friendly Version

Interactive Discussion



Idealized simulations of pyro-convective clouds

P. Reutter et al.

Title Page

Abstract

Introduction

Conclusions

References

Tables

Figures

◀

▶

◀

▶

Back

Close

Full Screen / Esc

Printer-friendly Version

Interactive Discussion



Arakawa, A. and Lamb, V. R.: Computational design of the basic dynamical processes of the ucla general circulation model, in: *General Circulation Models of the Atmosphere*, Academic Press, New York, 173–265, 1977. 19531

ASRD: Final Documentation Report – Chisholm Fire (LWF-063), Forest Protection Division, ISBN 0-7785-1841-8, Tech. rep., Alberta Sustainable Resource Development, 2001. 19533

Blahak, U.: Towards a better representation of high density ice particles in a state-of-the-art two-moment bulk microphysical scheme, in: *Proc. 15th Int. Conf. Clouds and Precip.*, Cancun, Mexico, 2008. 19532

Costa, A. A., de Oliveira, C. J., de Oliveira, J. C. P., and da Costa Sampaio, A. J.: Microphysical observation of warm cumulus clouds in Ceara, Brazil, *Atmos. Res.*, 54, 167–199, 2000. 19542

Cunningham, P. and Reeder, M. J.: Severe convective storms initiated by intense wildfires: Numerical simulations of pyro-convection and pyro-tornadogenesis, *Geophys. Res. Lett.*, 36, L12812, doi:10.1029/2009GL039262, 2009. 19530

Diehl, K., Simmel, M., and Wurzler, S.: Effects of drop freezing on microphysics of an ascending parcel under biomass burning conditions, *Atmos. Environ.*, 41, 303–314, 2007. 19542

Fromm, M. and Servranckx, R.: Transport of forest fire smoke above the tropopause by supercell convection, *Geophys. Res. Lett.*, 30, 142, doi:10.1029/2002GL016820, 2003. 19529

Fromm, M., Alfred, J., Hoppel, K., Hornstein, J., Bevilacqua, R., Shettle, E., Servranckx, R., Li, Z., and Stocks, B.: Observations of boreal forest fire smoke in the stratosphere by POAM III, SAGE II, and lidar in 1998, *Geophys. Res. Lett.*, 27, 9, 1407–1410, 2000. 19529

Fromm, M., Lindsey, D. T., Servranckx, R., Yue, G., Trickl, T., Sica, R., Doucet, P., and Godin-Beekmann, S.: The untold story of pyrocumulonimbus, *B. Am. Meteorol. Soc.*, 91, 9, 1193–1209, doi:10.1175/2010BAMS3004.1, 2010. 19529

Graf, H.-F., Herzog, M., Oberhuber, J. M., and Textor, C.: The effect of environmental conditions on volcanic plume rise, *J. Geophys. Res.*, 104, 24309–24320, 1999. 19531

Herzog, M., Graf, H.-F., and Oberhuber, J. M.: A prognostic turbulence scheme for the nonhydrostatic plume model ATHAM, *J. Atmos. Sci.*, 60, 2783–2796, 2003. 19531

Khain, A., Rosenfeld, D., and Pokrovsky, A.: Aerosol impact on the dynamics and microphysics of deep convective clouds, *Q. J. Roy. Meteorol. Soc.*, 131, 2639–2663, 2005. 19542

Koren, I., Kaufman, Y. J., Rosenfeld, D., Remer, L. A., and Rudich, Y.: Aerosol invigoration and restructuring of Atlantic convective clouds, *Geophys. Res. Lett.*, 32, L14828, doi:10.1029/2005GL023187, 2005. 19530

**Idealized simulations
of pyro-convective
clouds**

P. Reutter et al.

[Title Page](#)[Abstract](#)[Introduction](#)[Conclusions](#)[References](#)[Tables](#)[Figures](#)[◀](#)[▶](#)[◀](#)[▶](#)[Back](#)[Close](#)[Full Screen / Esc](#)[Printer-friendly Version](#)[Interactive Discussion](#)

- Lavoué, D., Lioussé, C., Cachier, H., Stocks, B. J., and Goldammer, J. G.: Modeling of carbonaceous particles emitted by boreal and temperate wildfires at northern latitudes, *J. Geophys. Res.*, 105, 26871–26890, 2000. 19530
- Lindsey, D. T. and Fromm, M.: Evidence of the cloud lifetime effect from wildfire-induced thunderstorms, *Geophys. Res. Lett.*, 35, L22809, doi:10.1029/2008GL035680, 2008. 19530
- Lohmann, U. and Feichter, J.: Global indirect aerosol effects: a review, *Atmos. Chem. Phys.*, 5, 715–737, doi:10.5194/acp-5-715-2005, 2005. 19532, 19534, 19540
- Luderer, G., Trentmann, J., Winterrath, T., Textor, C., Herzog, M., Graf, H. F., and Andreae, M. O.: Modeling of biomass smoke injection into the lower stratosphere by a large forest fire (Part II): sensitivity studies, *Atmos. Chem. Phys.*, 6, 5261–5277, doi:10.5194/acp-6-5261-2006, 2006. 19529, 19535
- Nedelec, P., Thouret, V., Brioude, J., Sauvage, B., Cammas, J.-P., and Stohl, A.: Extreme CO concentrations in the upper troposphere over northeast Asia in June 2003 from the in situ MOZAIC aircraft data, *Geophys. Res. Lett.*, 32, L14807, doi:10.1029/2005GL023141, 2005. 19529
- Noppel, H., Blahak, U., Seifert, A., and Beheng, K. D.: Simulations of a hailstorm and the impact of CCN using an advanced two-moment cloud microphysical scheme, *Atmos. Res.*, 96, 286–301, 2010. 19532
- Oberhuber, J., Herzog, M., Graf, H.-F., and Schwanke, K.: Volcanic plume simulation on large scales, *J. Volcanol. Geoth. Res.*, 87, 29–53, 1998. 19531
- Penner, J. E., Haselman, Jr., L. C., and Edwards, L. L.: Smoke-plume distribution above large-scale fires: implications for simulations of “nuclear winter”, *J. Clim. Appl. Meteorol.*, 25, 1434–1444, 1986. 19530
- Petters, M. D. and Kreidenweis, S. M.: A single parameter representation of hygroscopic growth and cloud condensation nucleus activity, *Atmos. Chem. Phys.*, 7, 1961–1971, doi:10.5194/acp-7-1961-2007, 2007. 19532
- Reid, J. S., Koppmann, R., Eck, T. F., and Eleuterio, D. P.: A review of biomass burning emissions part II: intensive physical properties of biomass burning particles, *Atmos. Chem. Phys.*, 5, 799–825, doi:10.5194/acp-5-799-2005, 2005. 19532
- Reutter, P., Su, H., Trentmann, J., Simmel, M., Rose, D., Gunthe, S. S., Wernli, H., Andreae, M. O., and Pöschl, U.: Aerosol- and updraft-limited regimes of cloud droplet formation: influence of particle number, size and hygroscopicity on the activation of cloud condensa-

Idealized simulations of pyro-convective clouds

P. Reutter et al.

Title Page

Abstract

Introduction

Conclusions

References

Tables

Figures

◀

▶

◀

▶

Back

Close

Full Screen / Esc

Printer-friendly Version

Interactive Discussion

tion nuclei (CCN), *Atmos. Chem. Phys.*, 9, 7067–7080, doi:10.5194/acp-9-7067-2009, 2009. 19531, 19532, 19541, 19547

Rosenfeld, D., Fromm, M., Trentmann, J., Luderer, G., Andreae, M. O., and Servranckx, R.: The Chisholm firestorm: observed microstructure, precipitation and lightning activity of a pyro-cumulonimbus, *Atmos. Chem. Phys.*, 7, 645–659, doi:10.5194/acp-7-645-2007, 2007. 19529

Rosenfeld, D., Lohmann, U., Raga, G. B., O'Dowd, C. D., Kulmala, M., Fuzzi, S., Reissell, A., and Andreae, M. O.: Flood or drought: how do aerosols affect precipitation?, *Science*, 321, 1309–1313, 2008. 19530, 19535

Seifert, A. and Beheng, K.: A two-moment cloud microphysics parameterization for mixed-phase clouds. Part II: Deep convective storms, *Meteorol. Atmos. Phys.*, 92, 67–88, 2006. 19532, 19540, 19542

Seifert, A., Köhler, C., and Beheng, K. D.: Aerosol-cloud-precipitation effects over Germany as simulated by a convective-scale numerical weather prediction model, *Atmos. Chem. Phys.*, 12, 709–725, doi:10.5194/acp-12-709-2012, 2012. 19542

Storer, R. L. and van den Heever, S. C.: Microphysical processes evident in aerosol forcing of tropical deep convective clouds, *J. Atmos. Sci.*, 70, 430–446, doi:10.1175/JAS-D-12-076.1, 2013. 19542

Tao, W.-K., Li, X., Khain, A., Matsui, T., Lang, S., and Simpson, J.: Role of atmospheric aerosol concentration on deep convective precipitation: cloud-resolving model simulations, *J. Geophys. Res.*, 112, D24S18, doi:10.1029/2007JD008728, 2007. 19542

Textor, C., Graf, H.-F., Herzog, M., Oberhuber, J. M., Rose, W. I., and Ernst, G. G. J.: Volcanic particle aggregation in explosive eruption columns part II: numerical experiments, *J. Volcanol. Geoth. Res.*, 150, 378–394, 2006. 19531

Trentmann, J., Luderer, G., Winterrath, T., Fromm, M. D., Servranckx, R., Textor, C., Herzog, M., Graf, H.-F., and Andreae, M. O.: Modeling of biomass smoke injection into the lower stratosphere by a large forest fire (Part I): reference simulation, *Atmos. Chem. Phys.*, 6, 5247–5260, doi:10.5194/acp-6-5247-2006, 2006. 19529, 19530, 19533

Tupper, A., Textor, C., Herzog, M., Graf, H.-F., Richards, M. S.: Tall clouds from small eruptions: the sensitivity of eruption height and fine ash content to tropospheric instability, *Nat. Hazards*, 51, 375–401, doi:10.1007/s11069-009-9433-9, 2009. 19531

Idealized simulations of pyro-convective clouds

P. Reutter et al.

Table 1. Number of cloud droplets in cm^{-3} for different cloud base updraft velocities w and initial aerosol concentration N_{CN} obtained from Reutter et al. (2009).

w, ms^{-1}	$N_{\text{CN}}, \text{cm}^{-3}$		
	1000	20 000	60 000
1.0	512.4	836.9	1242.5
2.5	836.9	2922.0	3795.0
5.0	914.6	7238.9	8902.5
7.0	930.9	10 114.0	12 841.7
10.0	940.1	13 250.5	17 931.7
12.0	942.2	14 525.0	21 165.6
15.0	942.9	15 993.8	25 273.8
17.0	943.0	16 478.9	27 534.8
20.0	942.9	17 212.9	30 375.9

Title Page

Abstract

Introduction

Conclusions

References

Tables

Figures

◀

▶

◀

▶

Back

Close

Full Screen / Esc

Printer-friendly Version

Interactive Discussion



Idealized simulations
of pyro-convective
clouds

P. Reutter et al.

Title Page

Abstract

Introduction

Conclusions

References

Tables

Figures

◀

▶

◀

▶

Back

Close

Full Screen / Esc

Printer-friendly Version

Interactive Discussion

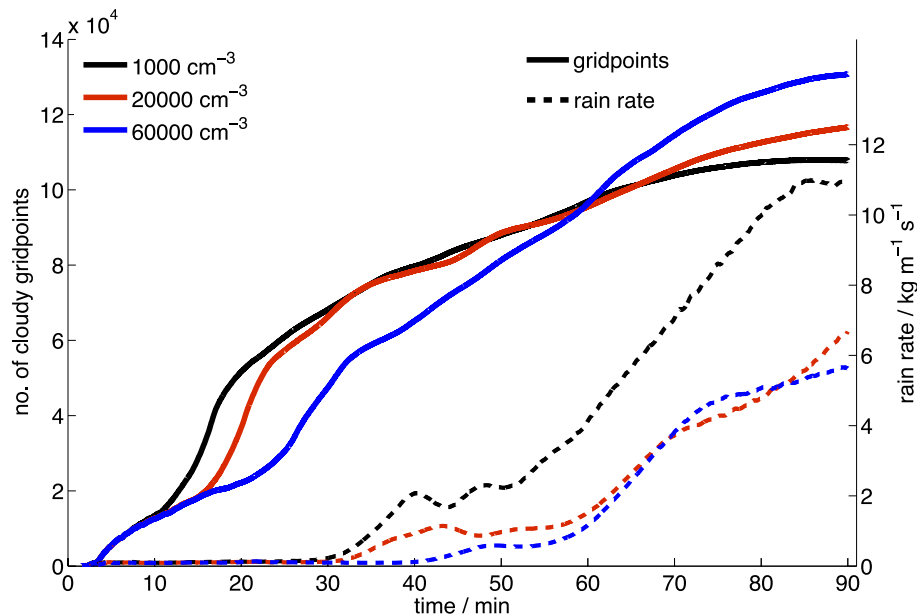


Fig. 1. Temporal evolution of (solid lines) the number of cloudy grid points for aerosol concentrations of (black) $N_{\text{CN}} = 1000 \text{ cm}^{-3}$, (red) $N_{\text{CN}} = 20000 \text{ cm}^{-3}$ and (blue) $N_{\text{CN}} = 60000 \text{ cm}^{-3}$ and (dashed) for the rain rate in $\text{kg m}^{-2} \text{ s}^{-1}$ of the three specified aerosol concentrations.

Idealized simulations
of pyro-convective
clouds

P. Reutter et al.

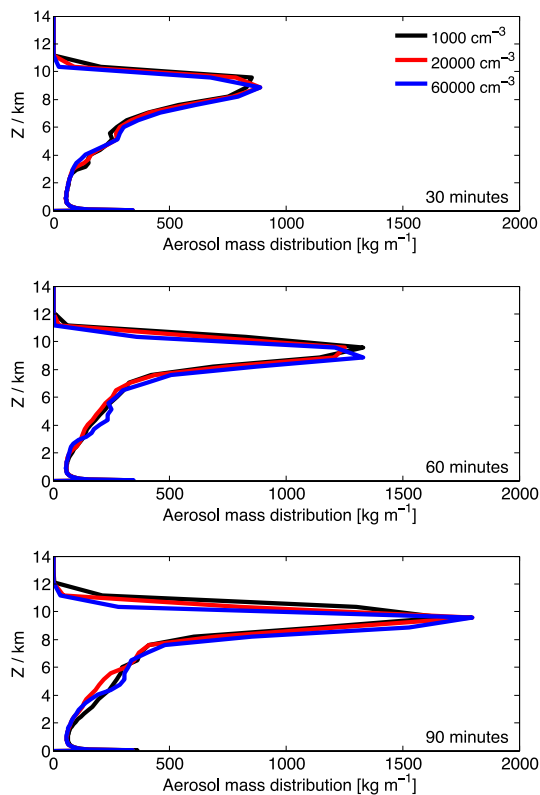


Fig. 2. Averaged vertical distribution of aerosol mass for (black) $N_{\text{CN}} = 1000 \text{ cm}^{-3}$, (red) $N_{\text{CN}} = 20000 \text{ cm}^{-3}$ and (blue) $N_{\text{CN}} = 60000 \text{ cm}^{-3}$ after 30, 60, and 90 min of simulation, respectively.

Title Page

Abstract

Introduction

Conclusions

References

Tables

Figures

◀

▶

◀

▶

Back

Close

Full Screen / Esc

Printer-friendly Version

Interactive Discussion



Idealized simulations of pyro-convective clouds

P. Reutter et al.

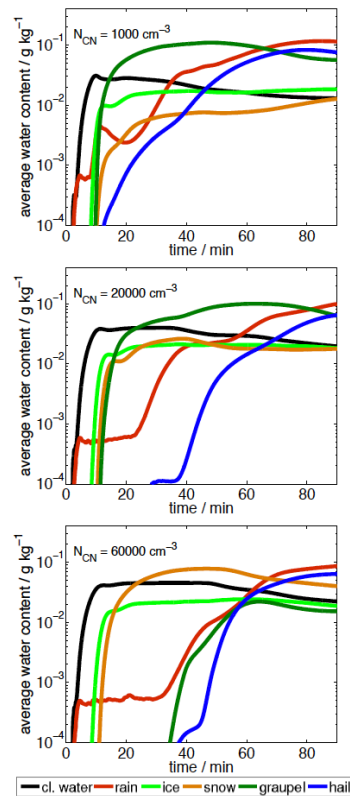


Fig. 3. Temporal evolution of the averaged water content [g kg^{-1}] in the model domain for the six hydrometeor classes (black) cloud water, (red) rain water, (green) ice, (orange) snow, (dark green) graupel and (blue) hail for (top) the clean case with $N_{\text{CN}} = 1000 \text{ cm}^{-3}$, (middle) the intermediate case with $N_{\text{CN}} = 20000 \text{ cm}^{-3}$ and (bottom) the strongly polluted case with $N_{\text{CN}} = 60000 \text{ cm}^{-3}$. The time axis ends after 90 min.

[Title Page](#)
[Abstract](#)
[Introduction](#)
[Conclusions](#)
[References](#)
[Tables](#)
[Figures](#)
[◀](#)
[▶](#)
[◀](#)
[▶](#)
[Back](#)
[Close](#)
[Full Screen / Esc](#)
[Printer-friendly Version](#)
[Interactive Discussion](#)


Idealized simulations of pyro-convective clouds

P. Reutter et al.

Title Page

Abstract

Introduction

Conclusions

References

Tables

Figures

◀

▶

◀

▶

Back

Close

Full Screen / Esc

Printer-friendly Version

Interactive Discussion

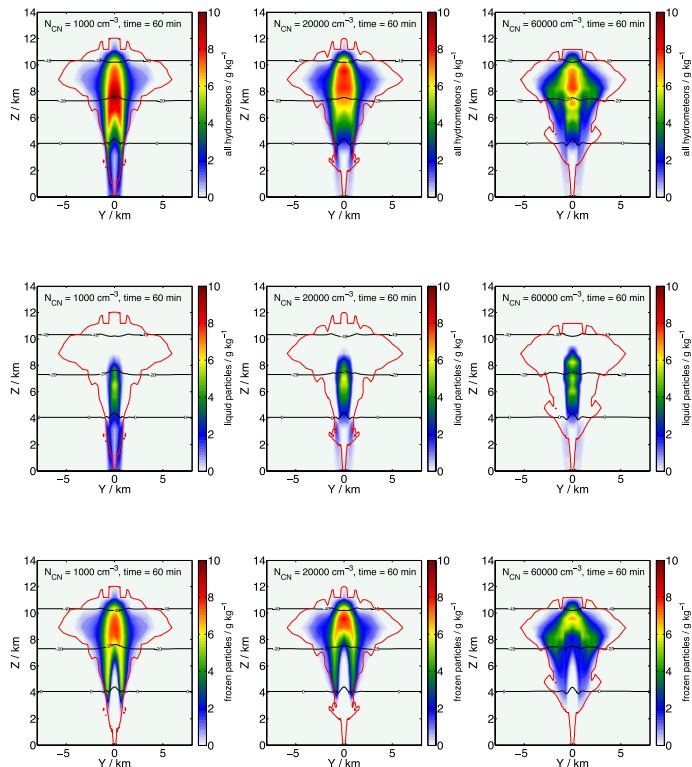


Fig. 4. Y-Z cross section at $x = 0$ km of (top row) the total hydrometeor water content in g kg^{-1} , (middle row) the liquid water content in g kg^{-1} and (bottom row) the frozen water content in g kg^{-1} after 60 min simulation time for (left) $N_{\text{CN}} = 1000 \text{ cm}^{-3}$, (middle) $N_{\text{CN}} = 20000 \text{ cm}^{-3}$ and (right) $N_{\text{CN}} = 60000 \text{ cm}^{-3}$. The black lines denote the 0°C , $0\text{--}20^\circ\text{C}$ and -40°C isothermes, respectively. The red line shows the $0.1 \mu\text{g kg}^{-1}$ isoline of the interstitial aerosol, which describes the shape of the smoke plume.

Idealized simulations
of pyro-convective
clouds

P. Reutter et al.

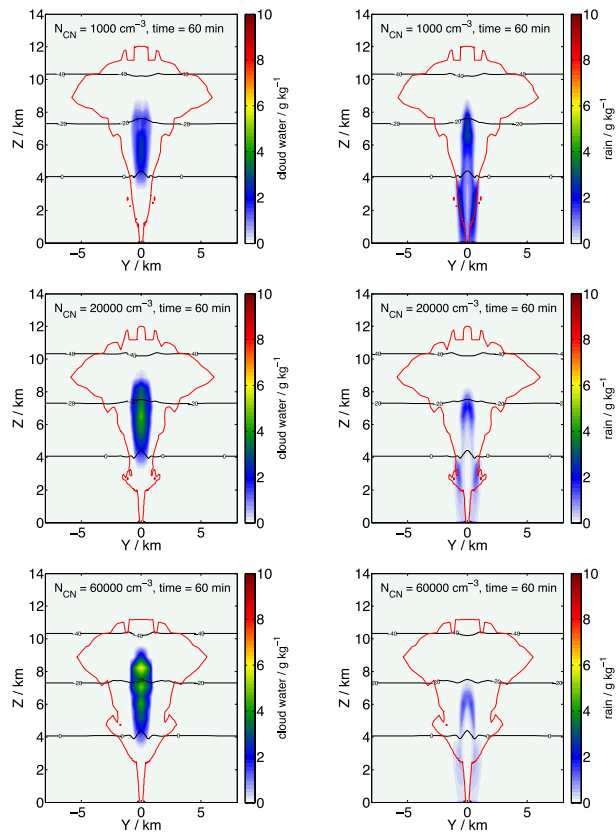


Fig. 5. Y-Z cross section at $x = 0$ km of the (left column) cloud water content in g kg^{-1} and (right column) rain water content in g kg^{-1} for (top row) the clean case, (middle row) the intermediate case and (bottom row) the strongly polluted case. The black lines denote the 0°C , $0\text{--}20^\circ\text{C}$ and -40°C isothermes, respectively. The red line shows the $0.1 \mu\text{g kg}^{-1}$ isoline of the interstitial aerosol.

Title Page

Abstract

Introduction

Conclusions

References

Tables

Figures

◀

▶

◀

▶

Back

Close

Full Screen / Esc

Printer-friendly Version

Interactive Discussion



Idealized simulations
of pyro-convective
clouds

P. Reutter et al.

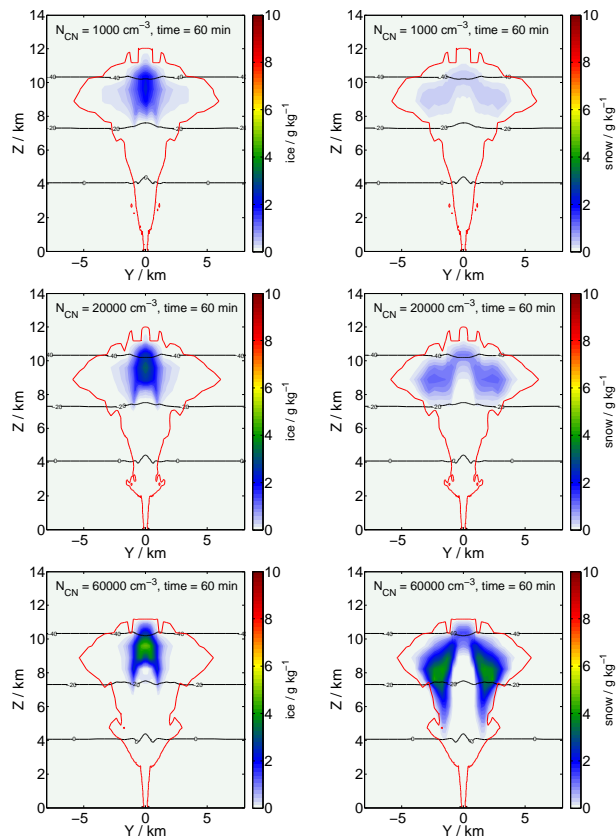


Fig. 6. Y-Z cross section at $x = 0 \text{ km}$ of the (left column) ice water content in g kg^{-1} and (right column) snow water content in g kg^{-1} for (top row) the clean case, (middle row) the intermediate case and (bottom row) the strongly polluted case. The black lines denote the 0°C, 0–20°C and -40°C isothermes, respectively. The red line shows the $0.1 \mu\text{g kg}^{-1}$ isoline of the interstitial aerosol.

Title Page

Abstract

Introduction

Conclusions

References

Tables

Figures

◀

▶

◀

▶

Back

Close

Full Screen / Esc

Printer-friendly Version

Interactive Discussion



Idealized simulations
of pyro-convective
clouds

P. Reutter et al.

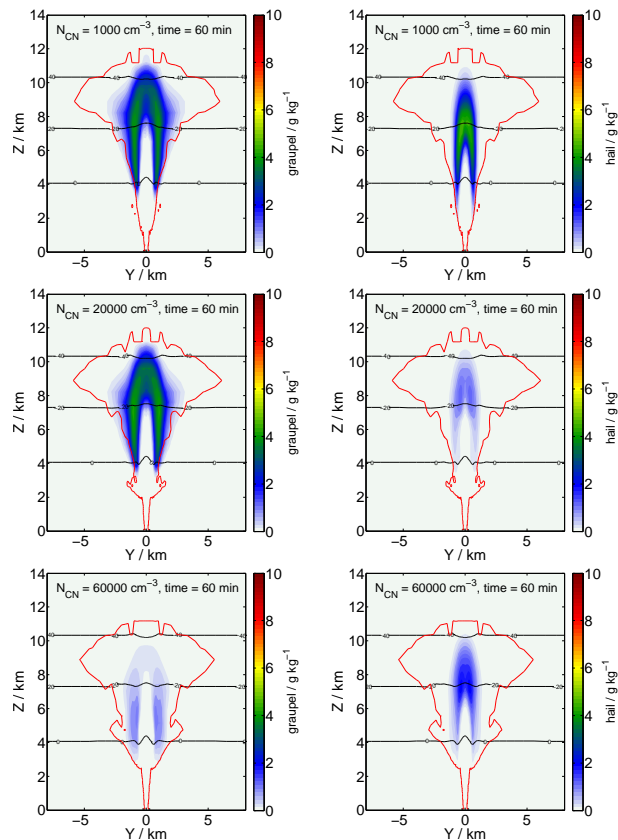


Fig. 7. Y-Z cross section at $x = 0 \text{ km}$ of the (left column) graupel water content in g kg^{-1} and (right column) hail water content in g kg^{-1} for (top row) the clean case, (middle row) the intermediate case and (bottom row) the strongly polluted case. The black lines denote the 0°C, 0–20°C and –40°C isotherms, respectively. The red line shows the 0.1 $\mu\text{g kg}^{-1}$ isoline of the interstitial aerosol.

Title Page

Abstract

Introduction

Conclusions

References

Tables

Figures

◀

▶

◀

▶

Back

Close

Full Screen / Esc

Printer-friendly Version

Interactive Discussion



Idealized simulations
of pyro-convective
clouds

P. Reutter et al.

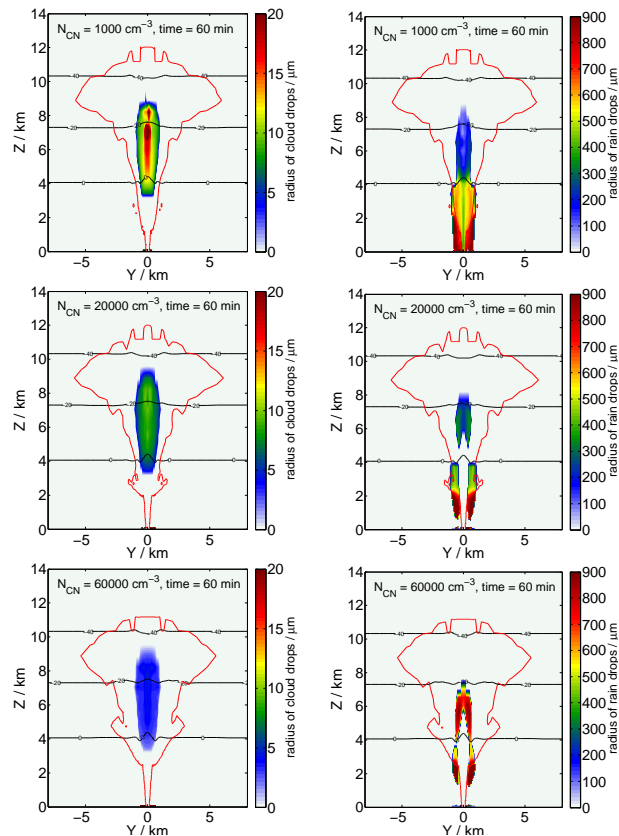


Fig. A1. Y-Z cross section at $x = 0 \text{ km}$ of the volume mean radius of (left column) cloud water content in μm and (right column) rain water content in μm for (top row) the clean case, (middle row) the intermediate case and (bottom row) the strongly polluted case. The black lines denote the 0°C , $0\text{--}20^\circ\text{C}$ and $\text{--}40^\circ\text{C}$ isotherms, respectively. The red line shows the $0.1 \mu\text{g kg}^{-1}$ isoline of the interstitial aerosol.

Idealized simulations
of pyro-convective
clouds

P. Reutter et al.

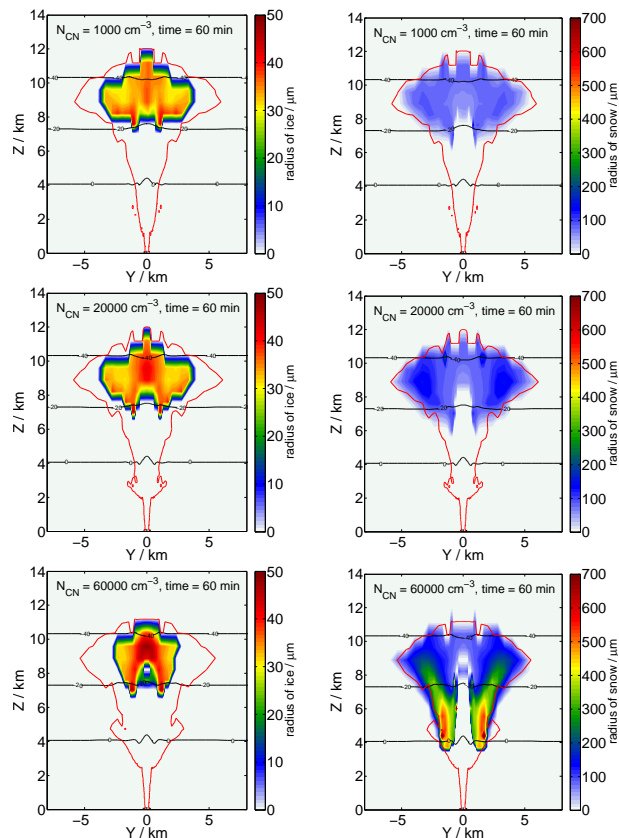


Fig. A2. Y-Z cross section at $x = 0\text{km}$ of the volume mean radius of (left column) ice water content in μm and (right column) snow water content in μm for (top row) the clean case, (middle row) the intermediate case and (bottom row) the strongly polluted case. The black lines denote the 0°C , $0-20^\circ\text{C}$ and -40°C isotherms, respectively. The red line shows the $0.1 \mu\text{g kg}^{-1}$ isoline of the interstitial aerosol.

Title Page

Abstract

Introduction

Conclusions

References

Tables

Figures

◀

▶

◀

▶

Back

Close

Full Screen / Esc

Printer-friendly Version

Interactive Discussion



Idealized simulations
of pyro-convective
clouds

P. Reutter et al.

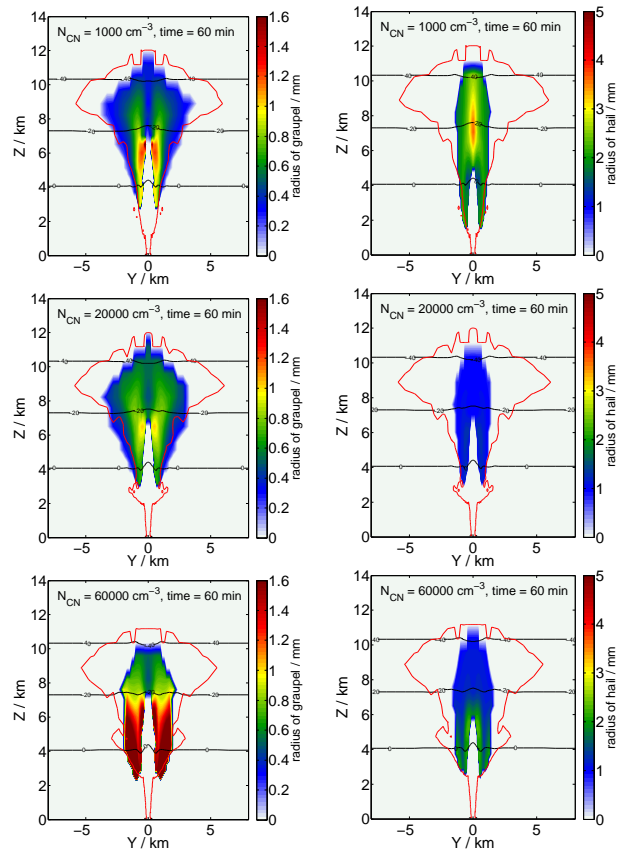


Fig. A3. Y-Z cross section at $x = 0 \text{ km}$ of the volume mean radius of (left column) graupel water content in μm and (right column) hail water content in μm for (top row) the clean case, (middle row) the intermediate case and (bottom row) the strongly polluted case. The black lines denote the 0°C , $0\text{--}20^\circ\text{C}$ and -40°C isotherms, respectively. The red line shows the $0.1 \mu\text{g kg}^{-1}$ isoline of the interstitial aerosol.

Title Page

Abstract

Introduction

Conclusions

References

Tables

Figures

◀

▶

◀

▶

Back

Close

Full Screen / Esc

Printer-friendly Version

Interactive Discussion